



You have downloaded a document from
RE-BUS
repository of the University of Silesia in Katowice

Title: Doubly Charged Higgs Bosons and Spontaneous Symmetry Breaking at eV and TeV Scales

Author: Janusz Gluza , Magdalena Kordiaczyńska, Tripurari Srivastava

Citation style: Gluza Janusz, Kordiaczyńska Magdalena, Srivastava Tripurari. (2020). Doubly Charged Higgs Bosons and Spontaneous Symmetry Breaking at eV and TeV Scales. "Symmetry" (2020, vol. 12, art. no. 153, p. 1-15), doi 10.3390/sym12010153



Uznanie autorstwa - Licencja ta pozwala na kopiowanie, zmienianie, rozprowadzanie, przedstawianie i wykonywanie utworu jedynie pod warunkiem oznaczenia autorstwa.



UNIwersYTET ŚLĄSKI
W KATOWICACH




Biblioteka
Uniwersytetu Śląskiego



Ministerstwo Nauki
i Szkolnictwa Wyższego

Article

Doubly Charged Higgs Bosons and Spontaneous Symmetry Breaking at eV and TeV Scales

Janusz Gluza ^{1,2} , Magdalena Kordiaczyńska ^{1,2,*} and Tripurari Srivastava ^{3,4}¹ Institute of Physics, University of Silesia, 40-007 Katowice, Poland; janusz.gluza@us.edu.pl² Faculty of Science, University of Hradec Králové, 500 03 Hradec Králové, Czech Republic³ Department of Physics, Indian Institute of Technology, Kanpur 208016, India; tripurari@prl.res.in⁴ Theoretical Physics Division, Physical Research Laboratory, Ahmedabad 380009, India

* Correspondence: mkordiaczynska@us.edu.pl

Received: 1 December 2019; Accepted: 7 January 2020; Published: 11 January 2020



Abstract: In this paper, beyond standard models are considered with additional scalar triplets without modification of the gauge group (Higgs Triplet Model—HTM) and with an extended gauge group $SU(2)_R \otimes SU(2)_L \otimes U(1)$ (Left–Right Symmetric Model—LRSM). These models differ drastically in possible triplet vacuum expectation values (VEV). Within the HTM, we needed to keep the triplet VEV at most within the range of GeV to keep the electroweak ρ parameter strictly close to 1, down to electronvolts due to the low energy constraints on lepton flavor-violating processes and neutrino oscillation parameters. For LRSM, the scale connected with the $SU(2)_R$ triplet is relevant, and to provide proper masses of non-standard gauge bosons, VEV should at least be at the TeV level. Both models predict the existence of doubly charged scalar particles. In this paper, their production in the e^+e^- collider is examined for making a distinction in the s- and t- channels between the two models in scenarios when masses of doubly charged scalars are the same.

Keywords: theoretical physics; particle physics; beyond Standard Model; scalar sector

1. Introduction

In 2012, the discovery of the neutral scalar particle, called the Higgs boson by the ATLAS [1] and CMS [2] collaborations, confirmed the mechanism of mass generation in the Standard Model (SM). However, SM can be an effective theory, similarly to as it was in the past with the Fermi four-interactions theory, and in particular, the scalar sector of the ultimate theory of elementary particles interactions may be more complex. One of the prime goals of Beyond Standard Model theories is a deeper understanding of neutrino tiny mass generation. An additional scalar triplet can explain the smallness of neutrino masses via the Type II seesaw mechanism. Also, there is a long-standing excess observed in anomalous magnetic moments of the muon which, if confirmed, cannot be explained within the Standard Model [3]. Furthermore, there are other phenomena in the universe which cannot be explained by the SM, that is, dark matter, baryon asymmetry, and dark energy, which call for the SM extensions and collider studies of possible exotic signals [4,5]. Extended scalar sectors include additional neutral and charged scalar particles. There are two ways to extend the scalar sector of the theory: directly, adding scalar fields, or indirectly, by extending the SM gauge group, which demands proper adjusting of the scalar sector. These additional particles can generate various lepton flavor and number violating processes, thus leaving signatures in the experiments. There are two facts which make them worth studying at colliders. Firstly, doubly charged scalars can produce the same sign dilepton signals at the colliders. Secondly, they are components of the triplet multiplets, an attractive scenario to explain neutrino masses. We focus on two popular models containing doubly charged scalars—SM with one extra triplet multiplet (HTM) and the left–right symmetric model (LRSM).

These two models exhibit two very different scales of spontaneous symmetry breaking scales—eV (HTM) and TeV (LRSM). Interestingly, though phenomenologically completely different, they can produce the same type of signatures at colliders when doubly charged scalars interact with leptons.

In this work, we focus on doubly charged scalar particle production in e^+e^- collisions within HTM and LRSM. Our main goal is to initialize the work in order to understand how both models can be differentiated when the doubly charged scalar $H^{\pm\pm}$ would be discovered. We discuss in detail relevant parameters of the model, carefully establishing benchmark points which give the same masses of $H^{\pm\pm}$ in both models, and analyze allowed scenarios for $H^{\pm\pm}$ decay branching ratios and possible $H^{\pm\pm}$ pair production in e^+e^- colliders.

1.1. Theoretical Introduction to HTM and LRSM

1.1.1. HTM

The HTM is one of the simplest extensions of the Standard Model. This model is based on the SM gauge group $SU(3)_C \times SU(2)_L \times U(1)_Y$. An additional $SU(2)_L$ scalar triplet is introduced in the particle content. We are following the convention $Y = 2Q - T_3$, where Q denotes the charge and T_3 is the third component of the isospin of the triplet. Depending on the hypercharge Y , the triplet contains neutral, singly- and doubly-charged scalars. In the studied case, the HTM's scalar sector is built of one scalar $SU(2)_L$ doublet Φ (in which the SM Higgs boson is situated) and the triplet Δ with $Y = 2$:

$$\Phi = \frac{1}{\sqrt{2}} \begin{pmatrix} \sqrt{2}w_\Phi^+ \\ v_\Phi + h_\Phi + iz_\Phi \end{pmatrix}, \quad \Delta = \frac{1}{\sqrt{2}} \begin{pmatrix} w_\Delta^+ & \sqrt{2}\delta^{++} \\ v_\Delta + h_\Delta + iz_\Delta & -w_\Delta^+ \end{pmatrix}. \quad (1)$$

where v_Φ and v_Δ denotes corresponding VEV, while w, h, z, δ are unphysical scalar fields. The physical singly charged state can be expressed by a combination of the doublet and triplet fields, where the doubly charged scalar field is already physical (see the Equations (A3a) and (A3c) in the Appendix A.1):

$$\begin{aligned} H^\pm &= -\sin\beta w_\Phi^\pm + \cos\beta w_\Delta^\pm, & \tan\beta &= \frac{\sqrt{2}v_\Delta}{v_\Phi}, \\ H^{\pm\pm} &= \delta^{\pm\pm}. \end{aligned} \quad (2)$$

The doublet and triplet VEVs v_Φ and v_Δ are bounded by the condition:

$$v = \sqrt{v_\Phi^2 + 2v_\Delta^2} \simeq 246 \text{ GeV}, \quad (3)$$

where v is the SM electroweak symmetry breaking scale.

In Appendix A.1, the other physical fields and their masses are presented. From those considerations and from the decay $h \rightarrow \gamma\gamma$, it is known that the $|M_{H^{\pm\pm}} - M_{H^\pm}|$ mass gap does not overstep ~ 50 GeV. That conclusion will be important for calculating the $H^{\pm\pm}$ decays and branching ratios.

In the HTM, we do not introduce the right-handed neutrino fields. Neutrinos get masses due to the Type II see-saw mechanism. As in the SM, left-handed leptons form doublets:

$$L_\ell = \begin{pmatrix} \nu_\ell \\ \ell \end{pmatrix}_L, \quad [\ell = e, \mu, \tau]. \quad (4)$$

Apart from the scalar potential presented in Appendix A.1, the Yukawa part of the Lagrangian should be added:

$$L_Y^\Delta = \frac{1}{2} h_{\ell\ell'} L_\ell^T C^{-1} i\sigma_2 \Delta L_{\ell'} + \text{h.c.} \quad (5)$$

where C is the charge conjugation operator and $h_{\ell\ell'}$ is the symmetric Yukawa matrix. The Yukawa lagrangian L_Y^Δ provides massive neutrinos and interaction between triplet fields and leptons, particularly the $H^{\pm\pm} - l^\mp - l'^\mp$ vertex. In this case, the Yukawa coupling [6] reads:

$$\mathcal{Y}_{\ell\ell'}^{\text{HTM}} = \frac{1}{\sqrt{2}v_\Delta} V_{PMNS}^* \text{diag}\{m_1, m_2, m_3\} V_{PMNS}^\dagger, \quad (6)$$

where m_i denotes neutrino masses, and the PMNS matrix V_{PMNS} is parametrized as follows:

$$V_{PMNS} = \begin{bmatrix} c_{12}c_{13}e^{i\alpha_1} & s_{12}c_{13}e^{i\alpha_2} & s_{13}e^{-i\delta_{CP}} \\ (-s_{12}c_{23} - c_{12}s_{23}s_{13}e^{i\delta_{CP}})e^{i\alpha_1} & (c_{12}c_{23} - s_{12}s_{23}s_{13}e^{i\delta_{CP}})e^{i\alpha_2} & s_{23}c_{13} \\ (s_{12}s_{23} - c_{12}c_{23}s_{13}e^{i\delta_{CP}})e^{i\alpha_1} & (-c_{12}s_{23} - s_{12}c_{23}s_{13}e^{i\delta_{CP}})e^{i\alpha_2} & c_{23}c_{13} \end{bmatrix}. \quad (7)$$

This vertex depends on the neutrino parameters, where introducing neutrino masses directly breaks the lepton number. In Section 1.2, we will analyze the impact of this vertex and the doubly charged scalar's contribution to the lepton-number-violating (LNV) and lepton-flavor-violating (LFV) processes. Note that this coupling is also inversely proportional to the triplet VEV v_Δ , so the constraint coming from LFV and LNV processes will also bound v_Δ .

1.1.2. LRSM

In the case of LRSM, the gauge group is extended by the $\mathbf{SU}(2)_R$ right-handed group, where it is now $SU(3)_C \otimes \mathbf{SU}(2)_R \otimes SU(2)_L \otimes U(1)_Y$ [7,8]. There are a few ways to break this gauge symmetry down to the electroweak scale. For that, new scalar multiplets are introduced. We are following [7–9] with the scalar sector constructed of one bidoublet and two triplets with $Y = 2$, one under the $SU(2)_L$ and one under the $SU(2)_R$ group:

$$\Delta_{L,R} = \frac{1}{\sqrt{2}} \begin{pmatrix} w_{\Delta_{L,R}}^+ & \sqrt{2}\delta_{L,R}^{++} \\ v_{\Delta_{L,R}} + h_{\Delta_{L,R}} + iz_{\Delta_{L,R}} & -w_{\Delta_{L,R}}^+ \end{pmatrix}. \quad (8)$$

Again, doubly charged scalar fields are obtained, which are already physical:

$$\begin{aligned} H_1^{++} &= \delta_L^{++}, \\ H_2^{++} &= \delta_R^{++}. \end{aligned} \quad (9)$$

For the decomposition of singly-charged and neutral ones, see [9]. The whole scalar sector consists of two types of doubly charged scalar particles, two singly charged scalars, three neutral scalars (apart from the SM Higgs particle), and two pseudoscalars. Their masses are analyzed in the Appendix A.2. The LRSM realises the Type I See-Saw Mechanism. Additional right-handed neutrino fields are also present here, and form both left- and right-handed lepton doublet multiplets under the $SU(2)_L$ and $SU(2)_R$ group, respectively:

$$L_{iL} = \begin{pmatrix} \nu'_i \\ l'_i \end{pmatrix}_L, \quad L_{iR} = \begin{pmatrix} \nu'_i \\ l'_i \end{pmatrix}_R. \quad (10)$$

This time, the Yukawa Lagrangian contains contributions from Δ_L and Δ_R [9]:

$$L_Y^l = -\bar{L}_R^c i\sigma_2 \Delta_L h_M L_L - \bar{L}_R^c i\sigma_2 \Delta_R h_M L_L + h.c., \quad (11)$$

and again, the $H_{1,2}^{\pm\pm} - l^\mp - l'^\mp$ vertex depends on heavy neutrino states masses and mixing. Since no explicit data for the mixing parameters of heavy neutrinos exists, we safely assumed that their couplings were diagonal (possible mixings are negligible for our scalar boson studies):

$$\mathcal{Y}_{\ell\ell'}^{\text{LRSM}} = \frac{1}{\sqrt{2}v_R} \text{diag}\{M_1, M_2, M_3\}. \tag{12}$$

1.2. LFV Bounds on the Triplets VEV

The $H^{\pm\pm} - l^\mp - l'^\mp$ vertex contributes to many LFV and LNV processes. In the Table 1 we present the most relevant processes with corresponding experimental limits. The theoretical formulas for branching ratios for low-energy processes used in this publication are [10]:

Table 1. Low-energy LFV processes with $H^{\pm\pm}$ mediation and corresponding experimental limits.

Process:	Diagrams:	Limits:
Radiative decay: $l \rightarrow l'\gamma$		$\text{BR}(\mu \rightarrow e\gamma) \leq 4.2 \times 10^{-13}$ [11] $\text{BR}(\tau \rightarrow e\gamma) \leq 3.3 \times 10^{-8}$ [12] $\text{BR}(\tau \rightarrow \mu\gamma) \leq 4.4 \times 10^{-8}$ [12]
Three body decay: $l \rightarrow l_1 l_2 l_3$		$\text{BR}(\mu \rightarrow eee) \leq 1.0 \times 10^{-13}$ [13] $\text{BR}(\tau \rightarrow l_1 l_2 l_3) \leq \sim 10^{-8}$ [14]
$\mu \rightarrow e$ conversion: $\mu N \rightarrow e N^*$		$R(\mu^- \text{Au} \rightarrow e^- \text{Au}) \leq 7.0 \times 10^{-13}$ [15]

$$\begin{aligned} \text{BR}(\mu \rightarrow e\gamma) &= \frac{\alpha_{em}}{192\pi} \frac{|\mathcal{Y}^\dagger \mathcal{Y}|_{e\mu}|^2}{G_F^2} \left(\frac{1}{M_{H^\pm}^2} + \frac{8}{M_{H^{\pm\pm}}^2} \right)^2 \text{BR}(\mu \rightarrow e\bar{\nu}_e\nu_\mu), \\ \text{BR}(\tau \rightarrow e\gamma) &= \frac{\alpha_{em}}{192\pi} \frac{|\mathcal{Y}^\dagger \mathcal{Y}|_{e\tau}|^2}{G_F^2} \left(\frac{1}{M_{H^\pm}^2} + \frac{8}{M_{H^{\pm\pm}}^2} \right)^2 \text{BR}(\tau \rightarrow e\bar{\nu}_e\nu_\tau), \\ \text{BR}(\tau \rightarrow \mu\gamma) &= \frac{\alpha_{em}}{192\pi} \frac{|\mathcal{Y}^\dagger \mathcal{Y}|_{\mu\tau}|^2}{G_F^2} \left(\frac{1}{M_{H^\pm}^2} + \frac{8}{M_{H^{\pm\pm}}^2} \right)^2 \text{BR}(\tau \rightarrow \mu\bar{\nu}_\mu\nu_\tau), \\ \text{BR}(\mu \rightarrow eee) &= \frac{1}{4G_F^2} \frac{|\mathcal{Y}^\dagger{}_{ee} \mathcal{Y}|_{\mu e}|^2}{M_{H^{\pm\pm}}^4} \text{BR}(\mu \rightarrow e\bar{\nu}_e\nu), \\ \text{BR}(\tau \rightarrow l_i l_j l_k) &= \frac{S}{4G_F^2} \frac{|\mathcal{Y}^\dagger{}_{\tau i} \mathcal{Y}|_{jk}|^2}{M_{H^{\pm\pm}}^4} \text{BR}(\tau \rightarrow \mu\bar{\nu}_\mu\nu), \quad S = \begin{cases} 1 & \text{if } j = k \\ 2 & \text{if } j \neq k \end{cases}. \end{aligned} \tag{13}$$

The rate of μ to e conversion in atomic nuclei [10,16,17] (Z_{eff} , Γ_{capt} and $F(q^2 \simeq -m_\mu^2)$) for the different atomic nuclei can be found in [18]:

$$\begin{aligned} R(\mu N \rightarrow e N^*) &= \frac{(\alpha_{em} m_\mu)^5 Z_{\text{eff}}^4 |F(q)|^2}{4\pi^4 m_{\Delta^{\pm\pm}}^4 \Gamma_{\text{capt}}} \times \left| \frac{\mathcal{Y}_{e\mu}^\dagger \mathcal{Y}_{\mu\mu}}{3} F(r, s_\mu) - \frac{3(\mathcal{Y}^\dagger \mathcal{Y})_{e\mu}}{8} \right|^2 \\ F(r, s_\mu) &= \ln s_\mu + \frac{4s_\mu}{r} + (1 - \frac{2s_\mu}{r}) \times \sqrt{1 + \frac{4s_\mu}{r}} \ln \frac{\sqrt{(1 + \frac{4s_\mu}{r}) + 1}}{\sqrt{(1 + \frac{4s_\mu}{r}) - 1}}, \\ r &= -\frac{q^2}{m_{\Delta^{\pm\pm}}^2}, s_\mu = \frac{m_\mu^2}{m_{\Delta^{\pm\pm}}^2}. \end{aligned} \tag{14}$$

The $H^{\pm\pm}$ and H^\pm contribution to the $(g - 2)_\mu$ process are presented by diagrams in Figure 1. The analytical formulas can be found in Equations (15) (Diagram I) and (16) (Diagrams II and III) [19,20]. By $q_{l/H}$ we denote the lepton/scalar charge, where $m_{l/H}$ is the mass of the lepton/scalar particle.

$$[\Delta a_\mu]_I = -q_l \frac{m_\mu^2 |\mathcal{Y}_{\mu l}|^2}{8\pi^2} \int_0^1 dx \left[\frac{\{x^2 - x^3 + \frac{m_l}{m_\mu} x^2\}}{(m_\mu^2 x^2 + (m_l^2 - m_\mu^2)x + M_H^2(1-x))} \right], \tag{15}$$

$$[\Delta a_\mu]_{II, III} = -q_H \frac{m_\mu^2 |\mathcal{Y}_{\mu l}|^2}{8\pi^2} \int_0^1 dx \left[\frac{\{(x^3 - x^2) + \frac{m_l}{m_\mu}(x^2 - x)\}}{(m_\mu^2 x^2 + (M_H^2 - m_\mu^2)x + (1-x)m_l^2)} \right]. \tag{16}$$

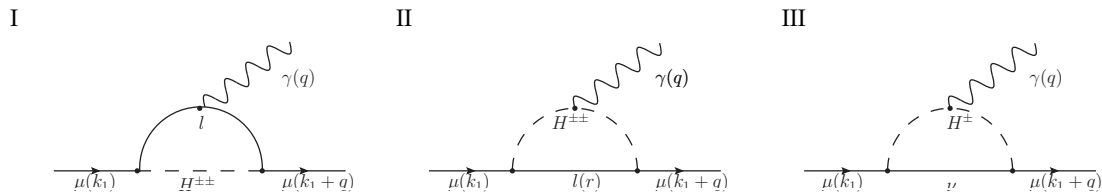


Figure 1. Singly- and doubly-charged scalars' contributions to $(g - 2)_\mu$.

2. A Case Study: Benchmark Points for the Scenario With $m_{H^{\pm\pm}} = 700$ GeV in HTM and LRSM

In this work, we examine the case when a mass of $H^{\pm\pm}$ is 700 GeV.

From the LHC data (see Figure 13 in [21]), to keep $M_{H^{\pm\pm}} \sim 700$ GeV, a doubly charged scalar's decays must satisfy the following conditions:

$$\begin{aligned} \text{BR}(H^{\pm\pm} \rightarrow ee) < 0.5 & \quad \text{BR}(H^{\pm\pm} \rightarrow \mu\mu) < 0.3, \\ \text{BR}(H^{\pm\pm} \rightarrow e\mu) < 0.5 & \quad \sum_{e,\mu} \text{BR}(H^{\pm\pm} \rightarrow ll') < 0.7. \end{aligned} \tag{17}$$

The above limits apply to the doubly charged scalar particles coupling to the left-handed leptons, but since in the LRSM we assume the degenerated case $M_{H_1^{\pm\pm}} = M_{H_2^{\pm\pm}}$, and the couplings $H_{1,2}^{\pm\pm} - l - l$ are equal, $H_2^{\pm\pm}$ has to fulfil the same condition. Those limits were calculated assuming that the doubly charged scalar particles decay 100% to leptons. In Section 3.2, we show that this assumption is justified both for HTM and LRSM. Relative leptonic branching ratios do not depend on the triplet VEV, but vary depending on neutrino parameters, as well as Majorana phases (see Figure 1 in [22]). For further calculation, we used the neutrino oscillation data from [23,24] within the 2σ confidence level range and Majorana phases $\alpha_{1,2} \in (0, 2\pi)$ (see the PMSN matrix parametrisation in Equation (7)).

In the case of LRSM, we covered the v_R region examined by the LHC with corresponding heavy neutrinos' masses [25,26]. Details are discussed in Section 3.1. Regarding the scalar particles' masses, we constructed a scalar mass spectrum in which $M_{H^{\pm\pm}} = 700$ GeV. Corresponding parameters of scalar potentials in both models are given in Table 2.

The mass benchmark points were constructed in order to satisfy several conditions.

For HTM, the potential stability imposed the following relation between the model parameters [27,28]:

$$\begin{aligned} \lambda \geq 0, \lambda_2 + \frac{\lambda_3}{2} \geq 0, \lambda_1 + \sqrt{\lambda(\lambda_2 + \lambda_3)} \geq 0, \lambda_1 + \lambda_4 + \sqrt{\lambda(\lambda_2 + \lambda_3)} \geq 0, \\ |\lambda_4| \sqrt{\lambda_2 + \lambda_3} - \lambda_3 \sqrt{\lambda} \geq 0 \quad \text{or} \quad 2\lambda_1 + \lambda_4 + \sqrt{(2\lambda\lambda_3 - \lambda_4^2)(\frac{2\lambda_2}{\lambda_3} + 1)} \geq 0. \end{aligned} \tag{18}$$

On the other hand, from unitarity constraints, we got [29,30]:

$$\begin{aligned} \text{Max} \left\{ \left| \frac{\lambda}{2} \right|, |\lambda_1|, \frac{1}{2} |2\lambda_1 + 3\lambda_4|, |\lambda_1 + \lambda_4|, \frac{1}{2} |2\lambda_1 - \lambda_4|, |\lambda_3 - 2\lambda_2|, |2\lambda_2|, \right. \\ \left. |2(\lambda_3 + \lambda_2)|, \frac{1}{4} \left| 3\lambda + 16\lambda_2 + 12\lambda_3 \pm \sqrt{(3\lambda - 16\lambda_2 - 12\lambda_3)^2 + 24(\lambda_4 + 2\lambda_1)^2} \right|, \right. \\ \left. \frac{1}{4} \left| \lambda + 4\lambda_2 + 8\lambda_3 \pm \sqrt{(\lambda - 4\lambda_2 - 8\lambda_3)^2 + 16\lambda_4^2} \right| \right\} \geq 16\pi (8\pi). \end{aligned} \tag{19}$$

Table 2. Exemplary benchmark points and corresponding potential parameters for HTM ($v_\Delta = 15$ eV) and LRSM ($v_R = 7000$ GeV) with $M_{H_{1,2}^{\pm\pm}} = 700$ GeV. The scalar potential parameters are defined in the Appendix A.1, Equations (A1) and (A6).

HTM	$\mu = 1.72 \times 10^{-7} \quad \lambda = 0.519 \quad \lambda_1 = 0.519 \quad \lambda_2 = 16.7 \quad \lambda_3 = 0. \quad \lambda_4 = 0.$					
	$M_h = 125$	$M_H = 700$	$M_{H^\pm} = 700$	$M_{H^{\pm\pm}} = 700$		
LRSM	$\lambda_1 = 0.129 \quad \rho_1 = 0.00375 \quad \rho_2 = 0.00375 \quad \rho_3 - 2\rho_1 = 0.015 \quad \alpha_3 = 4.0816 \quad 2\lambda_2 - \lambda_3 = 0$					
	$M_{H_0^0} = 125$	$M_{H_1^0} = 10\,000$	$M_{H_2^0} = 606$	$M_{H_3^0} = 606$		
	$M_{H_1^{\pm\pm}} = 700$	$M_{H_2^{\pm\pm}} = 700$	$M_{H_1^\pm} = 655$	$M_{H_2^\pm} = 10\,003$		

The right side of the above inequality depends on the convention, whether we chose the scattering matrix element \mathcal{M} less than 16π (what corresponds with the 0th partial wave amplitude $|a_0| \leq 1$, see Equation (1) in [30]) or 8π ($|\text{Re}(a_0)| \leq \frac{1}{2}$). Figure 2 in Reference [27] presents the mass region plot for heavy neutral scalar M_H and singly charged scalar M_{H^\pm} allowed from potential stability, unitarity, and the T parameter [31,32] for the triplet VEV 1 eV. The calculations for M_{H^\pm} and $M_{H^{\pm\pm}}$ in Figure 2 using both $\mathcal{M} < 16\pi$ and $\mathcal{M} < 8\pi$ constrained the maximum $|M_{H^{\pm\pm}} - M_{H^\pm}|$ gap, and thanks to that, we could determine possible $H^{\pm\pm}$ decay channels. The mass gap should be less than M_W . Taking those results into account, we found our choice of a degenerate mass case $M_{H^{\pm\pm}} = M_{H^\pm} = M_H$ fulfilled the potential stability, unitarity, and the T parameter restriction and bounds from $h \rightarrow \gamma\gamma$ [27,32–34].

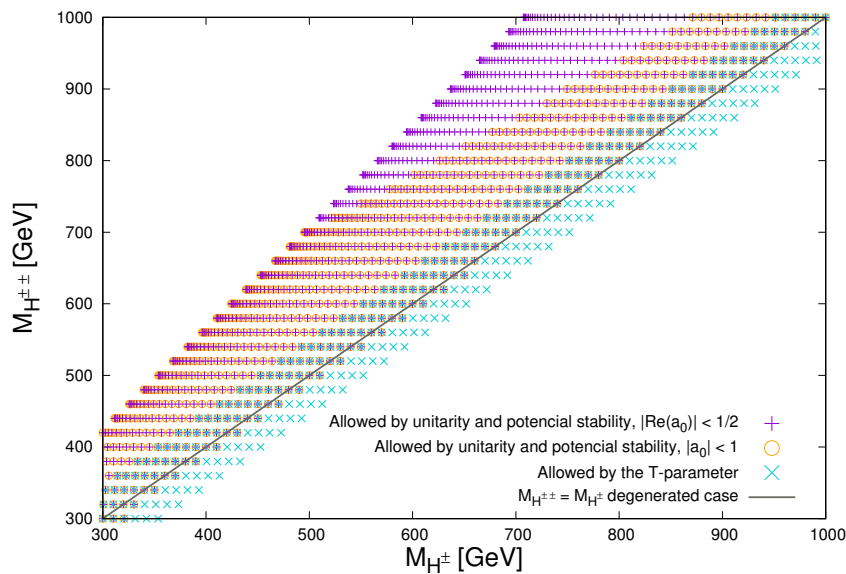


Figure 2. Singly and doubly charged scalars' mass dependence with limits coming from unitarity, potential stability, and the T parameter for $v_\Delta = 1$ eV.

3. Results and Discussion

In this section, we will apply determined parameters of the HTM and LRSM models and calculate possible VEV scales, and in order to compare the two models, the $H_{(1,2)}^{\pm\pm}$ branching ratios. In numerical calculations, fortran and Mathematica scripts were used, and the cross-section $e^+e^- \rightarrow H_{(1,2)}^{\pm\pm} H_{(1,2)}^{\mp\mp}$ process was calculated using MadGraph [35].

3.1. Limits on the Triplet VEV

The limits on the triplet VEVs come from several sources. Firstly, the additional scalar triplets under the $SU(2)_L$ group impact the value of the ρ parameter which relates masses of W and Z bosons with gauge SM gauge couplings [36] or gives a ratio of charged and neutral currents (see the Appendix in [37]). Taking experimental data into account, $\rho^{exp} = 1.00037 \pm 0.00023$, scalar triplet v_Δ is restricted from above, and the maximum VEV is of the order of 1.7 GeV. We assumed that for LRSM, the VEV of the $SU(2)_L$ scalar triplet is equal to zero. That choice allows for avoidance of the fine-tuning problem discussed in [8,38]. In HTM, the $SU(2)_L$ scalar triplet is restricted from the bottom by the low energy constraints, where it is not possible to set it to zero. In Table 3, we present the lowest limit on the HTM triplet VEV for $M_{H^{\pm\pm}} = 700$ GeV. The limits come from solutions to the relations in Equations (6) and (7), as well as experimental data on masses and mixing of neutrinos.

Table 3. Lower limits on the triplet vacuum expectation value v_Δ (in eV) for doubly charged scalar’s mass $M_{H^{\pm\pm}} = 700$ GeV. We calculated the above results by scanning through the entire space of neutrino oscillation parameters, that is, within a $\pm 2\sigma$ confidence level range of mixing parameters [23,24], as well as the whole range of Majorana phases $\alpha_{1,2}$, taking into account the cosmological neutrino mass limit $\sum_{i=1}^3 m_{\nu_i} < 0.23$ eV [39].

	NH	IH
min v_Δ [eV]	0.93	1.07

In the case of the $SU(2)_R$ scalar triplet VEV in LRSM, the ρ parameter was preserved if $v_R \gg \kappa_+$, where κ_+ is the SM electroweak symmetry breaking scale (see Equation (42) in [9]). On the other hand, to provide correct masses of heavy scalars and right-handed gauge bosons, v_R had to be at least at the TeV range. As we were interested in the region potentially examined by the LHC, we needed to restrict its value to the range $v_R \in 10^3 \div 10^4$ GeV. As the LNV and LFV bounds discussed in Section 1.2 depend on heavy neutrino masses, using the relation between the heavily charged gauge boson’s mass and $SU(2)_R$ triplet VEV:

$$M_{W_2}^2 \simeq \frac{g^2 v_R^2}{2} \Rightarrow M_{W_2} \simeq 0.47 v_R. \tag{20}$$

We were able to find the parameter space for the triplet VEV v_R and heavy neutrino masses. For that, we used the CMS experimental data from the $pp \rightarrow lljj$ process. Figure 6 in [25] and Figure 7 in [26] present $M_{W_2} - M_N$ exclusion plots, assuming $M_{W_2} > M_N$. For convenience, we repeat them here (see Figure 3). We used these data and exclusion plots for further analysis.

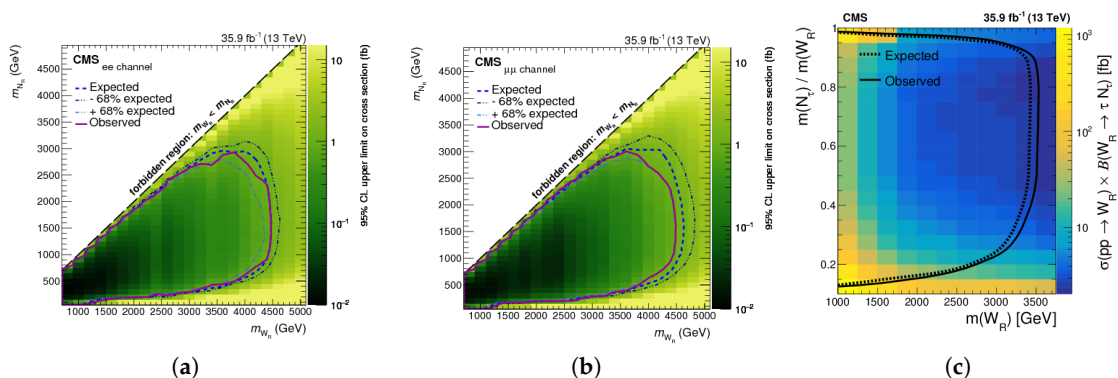


Figure 3. Upper limit on the $pp \rightarrow lljj$ cross-section for different and mass hypotheses, for the electron (a), muon (b), and taon (c) channels. The thin-dotted (blue) curves in the Figures (a) and (b) indicate the region in (M_{W_2}, M_{N_i}) parameter space that is expected to be excluded at 68% CL [25,26].

3.2. Doubly Charged Scalar Particles Decays within the LRSM and HTM

3.2.1. HTM

In the HTM model, the doubly charged scalar can decay to leptons, a W^\pm boson, and singly charged scalar particles. Because the singly and doubly charged scalars' mass gap is less than M_W , the $H^{\pm\pm} \rightarrow H^\pm H^\pm$ and $H^{\pm\pm} \rightarrow H^\pm W^\pm$ processes are suppressed. There are two possibilities left: $H^{\pm\pm} \rightarrow l_i^\pm l_j^\pm$ and $H^{\pm\pm} \rightarrow W^\pm W^\pm$. Since $H^{\pm\pm} - W^\pm - W^\pm$ is proportional to the triplet VEV v_Δ , and $H^{\pm\pm} - l_i^\pm - l_j^\pm \sim v_\Delta^{-1}$, leptonic channels dominate, from 0 up to $v_\Delta \sim 10^5$ eV (see Figure 4 in [40]), so our assumption that doubly charged particles decay purely to leptons is valid for our benchmark points, especially when we are interested in the low v_Δ values at the range of $1 \div 10$ eV.

3.2.2. LRSM

In the LRSM, the doubly charged scalar particles can decay to gauge bosons W_1, W_2 , and singly charged scalars H_1^\pm and H_2^\pm . Some of those decays are connected with vertices which are proportional to the $SU(2)_L$ triplet VEV $v_L = 0$ or to the $W_1 - W_2$ mixing angle $\xi \lesssim 10^{-2}$ [41,42]. Also, as $M_{H_{1,2}^{\pm\pm}} \ll M_{H_1^\pm}$ (see Equation (A8h)) and $M_{H_{1,2}^{\pm\pm}} \ll M_{W_2}$, diagrams involving heavy gauge bosons are suppressed for the 1.5 TeV e^+e^- collision energy, again, leptonic decays of doubly charged scalar particles dominate.

3.3. Doubly Charged Scalar Particles' Pair Production at Future High Energies

Let us consider the potential production of the doubly charged scalar particle pair at a e^+e^- collision energy of 1.5 TeV. A TeV energy range of e^+e^- colliders has been studied intensively in the past. Presently, the only considered scenario with such extreme collision energies of leptons is the CLIC project [43] (in future, extreme energies may become possible in Plasma Wakefield Linear Colliders [44]). The list of Feynman diagrams is given in Figure 4. In the s-channel, a $H^{\pm\pm}$ pair production goes by scalar and gauge bosons (Figure 4a), and in the t-channel, production is connected with an exchange of the charged lepton (Figure 4b).

For the s-channel, in two considered models, the photon, Z boson, and SM-like Higgs particles contribute. In HTM, additional scalar H can also couple to leptons and doubly charged scalar particles, where in LRSM, H_1^0 and H_2^0 also contribute. Examining couplings carefully, we can find that the scalars' contribution to this process is negligible. In LRSM the heavy gauge Z_2 boson is also present in the s-channel.

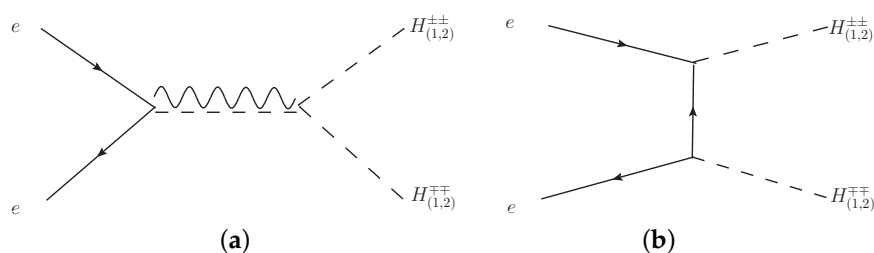


Figure 4. Feynman diagrams for the (a) s-channel and (b) t-channel pair production of doubly charged scalar particles in the e^+e^- collision. The following particles contribute to the diagrams: HTM: γ, Z, h and H (s-channel); e, μ, τ (t-channel). LRSM: $\gamma, Z_1, Z_2, H_0^0, H_1^0, H_2^0$ (s-channel); e (t-channel). The LFV breaking vertex $H_{1,2}^{\pm\pm} - l_i - l_j$ is not present since Yukawa couplings are assumed to be diagonal (see Equation (12)).

The t-channel diagram contains the $H_{(1,2)}^{\pm\pm} - l - l'$ vertex, which depends on the triplet VEV (see Equations (6) and (12)). Figure 5 presents the cross-section for the $e^+e^- \rightarrow H_{(1,2)}^{\pm\pm} H_{(1,2)}^{\mp\mp}$ process and its dependence on the triplet VEVs within the HTM (left) and LRSM (right) models.

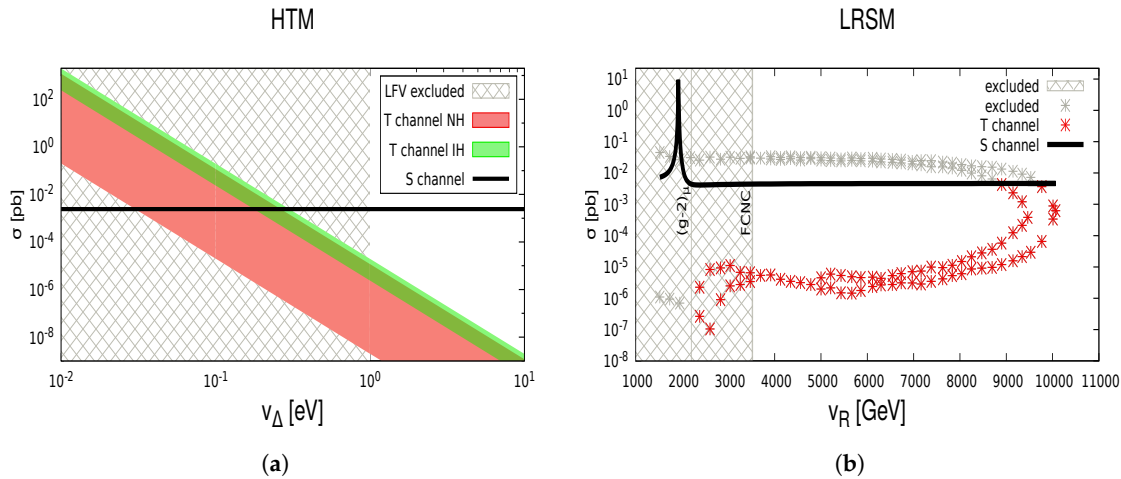


Figure 5. Doubly charged particles' pair production $e^+e^- \rightarrow H^{++}H^{--}$ for $M_{H_{(1,2)}^{\pm\pm}} = 700$ GeV and CM energy 1.5 TeV. (a) Left figure is for the HTM and (b) LRSM. The choice of the parameter space is discussed in Sections 2 and 3.1. The crossed area is excluded by (a) the LFV processes (b) and $(g-2)_\mu$ and FCNC. The maximum for $v_R = 1900$ GeV comes from the Z_2 resonance.

As expected, the t-channel dominates for the lower triplet VEV v_Δ . The shaded regions correspond to normal (red area) and inverted (green area) neutrino mass hierarchies, with neutrino parameters smeared within $\pm 2\sigma$ for Majorana phases $\alpha_{1,2} \in (0, 2\pi)$, taking into account the cosmological neutrino mass limit $\sum m_{\nu_i} < 0.23$ eV [39]. On the other hand, taking into account LFV processes and limits given in Table 3, we can see that triplet VEV $v_\Delta < 1$ eV is forbidden by the low energy experiments, so the whole region where the t-channel could bring a significant contribution is excluded.

In LRSM, we studied possible triplet VEV values using LHC CMS data for possible heavy neutrino masses N_e, N_μ and N_τ within the 68% confidence level, assuming $M_{W_2} > M_{N_i}$ (see Figure 3). The result is given in Figure 5b). We assumed diagonal Yukawa couplings and no LFV in the $H_{1,2}^{\pm\pm} - l - l$ vertex. Still, additional constraints came from experimental data which was discussed in Section 1.2, such as couplings \mathcal{Y}_{ee} and $\mathcal{Y}_{\mu\mu}$ couplings which was a constraint by the $(g-2)_\mu$ experiment (see Equations (15) and (16)), $e^+e^- \rightarrow l^+l^-$ [45], and the Møller scattering [46]. Both branching ratios Equation (17) and FCNC limits on the scalar particles masses were also crucial in our analysis (see Appendix A.1).

Taking the above bounds into account, we excluded the triplet VEV below ~ 3600 GeV and the parameter region where the t-channel could dominate over the s-channel. However, in contrast to the HTM model, the t-channel's contribution is still comparable with the s-channel, and cannot be neglected.

Regarding the s-channels, both in HTM and LRSM, this channel does not depend on the triplet VEV, and a significant Z_2 contribution is excluded by the $(g-2)_\mu$ and FCNC conditions, so a heavy gauge boson contribution does not affect the final results for the s-channel contributions and $H_{(1,2)}^{++} H_{(1,2)}^{--}$ pair production.

Here, we have focused on the $H^{\pm\pm}$ pair production process in e^+e^- collisions. As signals might be observable at some regions of model parameters, in future we plan to carefully study subsequent decays of $H^{\pm\pm}$, as well as background processes. It is worth noticing that doubly charged scalars can exhibit small decay widths, thus having long life-spans [47,48], and they do not leave any signatures in the detector-charged tracker, or can even escape the detector. However, they can deposit energy on different sub-detectors. Thus, they can be searched for through displaced secondary vertices analysis.

This kind of search can be important for feeble interactions of doubly charged scalars, and can be complementary to same-sign dilepton decay studies of doubly charged scalars with prompt decays. Studying such scenarios is also on our agenda. Searches for heavy long-lived multi-charged particles have already been initiated by many collider experiments, such as ATLAS, CMS, and Tevatron [49–52].

4. Summary and Outlook

In this article, we have discussed the present status of the simplest beyond-SM models which include doubly charged scalar particles. We presented the status of experimental data relevant for the determination of non-standard spontaneous symmetry breaking and VEVs in both models. We made a case study for a realistic scenario when a mass of this particle is 700 GeV, taking into account all relevant experimental constraints, and discussed its decay channels and a possibility of $H^{\pm\pm}$ pair production in future e^+e^- colliders, as a function of allowed VEV. In HTM, the low-energy experiments, such as $(g-2)_\mu$, ρ -parameter, and LFV and LNV processes put stringent constraints over triplet VEV such that $v_\Delta \lesssim \mathcal{O}(\text{eV})$, whereas right-handed triplet VEV in LRSM was constrained by the search for the new charged gauge boson which required $v_R \gtrsim \mathcal{O}(\text{TeV})$, depending on the mass of right-handed heavy neutrinos. We provided the benchmark for both the models considering the mass of a doubly charged scalar to be 700 GeV. In the proposed e^+e^- colliders, the doubly charged scalar can be produced in pairs via the Drell-Yan process, heavy neutral bosons, and BSM neutral scalars. In HTM, pair production is dominated by the t-channel in region $v_\Delta \gtrsim \mathcal{O}(\text{eV})$, which is excluded by the low energy experiments. In LRSM, the right-handed breaking scale $v_R < 3600 \text{ GeV}$ is excluded by low energy constraints, including FCNC, but the t-channel can still be comparable with the s-channel, and provides appreciable contribution to the doubly charged scalar pair production, in contrast to HTM. The s-channel contribution to the pair production process is, however, practically the same in both models for the considered realistic benchmarks. Therefore, the conclusion is that the signals are more promising in the case of LRSM, where the t-channel can be comparable with s-channel contributions for v_R values up to 10 TeV. We plan to study such cases more carefully in the future, paying more attention to the decay modes, background processes, and scenarios with displaced vertices. However, a more relevant option in the context of our studies seems to be pp colliders, HL-LHC, and particularly, the FCC-hh collider, which opens up the window for huge energies of proton–proton collisions up to 100 TeV [4,5,53].

Author Contributions: Conceptualization, investigation, methodology, resources: J.G., M.K. and T.S.; software, validation: M.K. and T.S.; writing, editing: J.G. and M.K.; visualization: M.K. and T.S.; supervision, project administration: J.G.; funding acquisition: J.G. and M.K. All authors have read and agreed to the published version of the manuscript.

Funding: This research was funded by the Polish National Science Center (NCN) under grant 2015/17/N/ST2/04067, the international mobilities for research activities of the University of Hradec Králové, CZ.02.2.69/0.0/0.0/16 027/0008487 and by COST (European Cooperation in Science and Technology) Action CA16201 PARTICLEFACE.

Acknowledgments: We thank Joydeep Chakraborty and Dipankar Das for useful discussions.

Conflicts of Interest: The authors declare no conflict of interest.

Abbreviations

The following abbreviations are used in this manuscript:

SM	Standard Model
HTM	Higgs Triplet Model
LRSM	left–right Symmetric Model
VEV	Vacuum Expectation Value
NH	Normal Hierarchy of neutrino masses
IH	Inverted Hierarchy of neutrino masses
LNV	Lepton Number Violation
LFV	Lepton flavor Violation

Appendix A

Appendix A.1. Scalar Particles within the HTM

The most general scalar potential with an additional triplet has the following form [29]:

$$V = -m_{\Phi}^2 (\Phi^\dagger \Phi) + \frac{\lambda}{4} (\Phi^\dagger \Phi)^2 + M_{\Delta}^2 \text{Tr} (\Delta^\dagger \Delta) + [\mu (\Phi^T i \sigma_2 \Delta^\dagger \Phi) + \text{h.c.}] + \lambda_1 (\Phi^\dagger \Phi) \text{Tr} (\Delta^\dagger \Delta) + \lambda_2 [\text{Tr} (\Delta^\dagger \Delta)]^2 + \lambda_3 \text{Tr} [(\Delta^\dagger \Delta)^2] + \lambda_4 \Phi^\dagger \Delta \Delta^\dagger \Phi, \quad (\text{A1})$$

where:

$$m_{\Phi}^2 = \frac{\lambda}{4} v_{\Phi}^2 + \frac{(\lambda_1 + \lambda_4)}{2} v_{\Delta}^2 - \sqrt{2} \mu v_{\Delta}, \quad (\text{A2a})$$

$$M_{\Delta}^2 = -(\lambda_2 + \lambda_3) v_{\Delta}^2 - \frac{(\lambda_1 + \lambda_4)}{2} v_{\Phi}^2 + \frac{\mu}{\sqrt{2}} \frac{v_{\Phi}^2}{v_{\Delta}}. \quad (\text{A2b})$$

The physical fields and their masses are:

$$H^{\pm\pm} = \delta^{\pm\pm} \quad (\text{A3a})$$

$$\begin{pmatrix} G_0 \\ A \end{pmatrix} = \begin{pmatrix} \cos \beta' & \sin \beta' \\ -\sin \beta' & \cos \beta' \end{pmatrix} \begin{pmatrix} z_{\Phi} \\ z_{\Delta} \end{pmatrix}, \quad \tan \beta' = \frac{2v_{\Delta}}{v_{\Phi}}, \quad (\text{A3b})$$

$$\begin{pmatrix} G^{\pm} \\ H^{\pm} \end{pmatrix} = \begin{pmatrix} \cos \beta & \sin \beta \\ -\sin \beta & \cos \beta \end{pmatrix} \begin{pmatrix} w_{\Phi}^{\pm} \\ w_{\Delta}^{\pm} \end{pmatrix}, \quad \tan \beta = \frac{\sqrt{2}v_{\Delta}}{v_{\Phi}}, \quad (\text{A3c})$$

$$\begin{pmatrix} h \\ H^0 \end{pmatrix} = \begin{pmatrix} \cos \alpha & \sin \alpha \\ -\sin \alpha & \cos \alpha \end{pmatrix} \begin{pmatrix} h_{\Phi} \\ h_{\Delta} \end{pmatrix}, \quad \tan 2\alpha = \frac{2B_S}{C_S - A_S}. \quad (\text{A3d})$$

$$M_{H^{\pm}}^2 = \frac{(2\sqrt{2}\mu - \lambda_4 v_{\Delta})}{4v_{\Delta}} (v_{\Phi}^2 + 2v_{\Delta}^2), \quad (\text{A4a})$$

$$M_{H^{\pm\pm}}^2 = \frac{\mu v_{\Phi}^2}{\sqrt{2}v_{\Delta}} - \frac{\lambda_4}{2} v_{\Phi}^2 - \lambda_3 v_{\Delta}^2, \quad (\text{A4b})$$

$$M_A^2 = \frac{\mu}{\sqrt{2}v_{\Delta}} (v_{\Phi}^2 + 4v_{\Delta}^2), \quad (\text{A4c})$$

$$M_h^2 = \frac{1}{2} \left((A_S + C_S) - \sqrt{(A_S - C_S)^2 + 4B_S^2} \right), \quad (\text{A4d})$$

$$M_{H^0}^2 = \frac{1}{2} \left((A_S + C_S) + \sqrt{(A_S - C_S)^2 + 4B_S^2} \right). \quad (\text{A4e})$$

where:

$$A_S = \frac{\lambda v_{\Phi}^2}{2}, \quad (\text{A5a})$$

$$B_S = \sqrt{2} \mu v_{\Phi} - (\lambda_1 + \lambda_4) v_{\Delta} v_{\Phi}, \quad (\text{A5b})$$

$$C_S = \frac{\mu v_{\Phi}^2}{\sqrt{2}v_{\Delta}} + 2(\lambda_2 + \lambda_3) v_{\Delta}^2. \quad (\text{A5c})$$

We are following the notation from [29]. We express the lagrangian coefficients λ, λ_i, μ (see Equation (A1)) as the functions of scalar particles' masses:

$$\lambda_1 = -\frac{2}{v_\Phi^2 + 4v_\Delta^2} M_A^2 + \frac{4}{v_\Phi^2 + 2v_\Delta^2} M_{H^\pm}^2 + \frac{\sin 2\alpha}{2v_\Phi v_\Delta} (M_h^2 - M_H^2), \quad (\text{A6a})$$

$$\lambda_2 = \frac{1}{v_\Delta^2} \left\{ \frac{s_\alpha^2 M_h^2 + c_\alpha^2 M_H^2}{2} + \frac{1}{2} \frac{v_\Phi^2}{v_\Phi^2 + 4v_\Delta^2} M_A^2 - \frac{2v_\Phi^2}{v_\Phi^2 + 2v_\Delta^2} M_{H^\pm}^2 + M_{H^{\pm\pm}}^2 \right\} \quad (\text{A6b})$$

$$\lambda_3 = \frac{1}{v_\Delta^2} \left\{ \frac{-v_\Phi^2}{v_\Phi^2 + 4v_\Delta^2} M_A^2 + \frac{2v_\Phi^2}{v_\Phi^2 + 2v_\Delta^2} M_{H^\pm}^2 - M_{H^{\pm\pm}}^2 \right\} \quad (\text{A6c})$$

$$\lambda_4 = \frac{4}{v_\Phi^2 + 4v_\Delta^2} M_A^2 - \frac{4}{v_\Phi^2 + 2v_\Delta^2} M_{H^\pm}^2 \quad (\text{A6d})$$

$$\lambda = \frac{2}{v_\Phi^2} \left\{ c_\alpha^2 M_h^2 + s_\alpha^2 M_H^2 \right\}, \quad (\text{A6e})$$

$$\mu = \frac{\sqrt{2}v_\Delta}{v_\Phi^2 + 4v_\Delta^2} M_A^2, \quad (\text{A6f})$$

where s_α and c_α denote $\sin \alpha$ and $\cos \alpha$ (Equations (A3d) and (A5)). We used an approximation $s_\alpha = \sin \alpha \sim 2\frac{v_\Delta}{v} \rightarrow 0$ [27]. Substituting the potential parameters in Equation (A4) by Equation (A6), relations between masses of physical states are obtained. They are not independent, and we chose $M_{H^{\pm\pm}}$, M_H and $M_h = 125$ GeV as external parameters for M_{H^\pm} and M_A :

$$M_A = \sqrt{\frac{(v_\Phi^2 + 4v_\Delta^2)(M_H^2 c_\alpha^2 + M_h^2 s_\alpha^2 - v_\Delta^2)}{v_\Phi^2}}, \quad (\text{A7a})$$

$$M_{H^\pm} = \sqrt{\frac{\left(M_{H^{\pm\pm}}^2 + \frac{v_\Phi^2 M_A^2}{v_\Phi^2 + 4v_\Delta^2} - v_\Delta^2\right) (v_\Phi^2 + 2v_\Delta^2)}{2v_\Phi^2}} \quad (\text{A7b})$$

Appendix A.2. The Mass Spectrum in LRSM

The scalar potential for LRSM with one bidoublet and two triplets is given in Equation (25) in [9]. Scalar particles masses as functions of potential parameters are presented in Equation (A8).

$$M_{H_0^0}^2 \simeq 2\kappa_+^2 \lambda_1 = 125 \text{ GeV} \quad (\text{A8a})$$

$$M_{H_1^0}^2 \simeq \frac{1}{2} \alpha_3 v_R^2 \geq 10 \text{ TeV} \quad (\text{A8b})$$

$$M_{H_2^0}^2 \simeq 2\rho_1 v_R^2 \quad (\text{A8c})$$

$$M_{H_3^0}^2 \simeq \frac{1}{2} v_R^2 (\rho_3 - 2\rho_1) \geq 55.4 \text{ GeV} \quad (\text{A8d})$$

$$M_{A_1^0}^2 \simeq \frac{1}{2} \alpha_3^2 v_R^2 - 2\kappa_+^2 (2\lambda_2 - \lambda_3) \geq 10 \text{ TeV} \quad (\text{A8e})$$

$$M_{A_2^0}^2 \simeq \frac{1}{2} v_R^2 (\rho_3 - 2\rho_1) \quad (\text{A8f})$$

$$M_{H_1^\pm}^2 \simeq \frac{1}{2} v_R^2 (\rho_3 - 2\rho_1) + \frac{1}{4} \alpha_3 \kappa_+^2 \geq 10 \text{ TeV} \quad (\text{A8g})$$

$$M_{H_2^\pm}^2 \simeq \frac{1}{2} \alpha_3 \left[v_R^2 + \frac{1}{2} \kappa_+^2 \right] \quad (\text{A8h})$$

$$M_{H_1^{\pm\pm}}^2 \simeq \frac{1}{2} \left[v_R^2 (\rho_3 - 2\rho_1) + \alpha_3 \kappa_+^2 \right] \quad (\text{A8i})$$

$$M_{H_2^{\pm\pm}}^2 \simeq 2\rho_2 v_R^2 + \frac{1}{2} \alpha_3 \kappa_+^2 \quad (\text{A8j})$$

where $k_+ = 246$ GeV is a combination of bidoublet VEVs. H_0^0 corresponds with the SM Higgs boson, so it has a mass of 125 GeV. Neutral H_1^0 and A_1^0 particles intermediate the Flavor-Changing Neutral Current (FCNC) processes [54], so their masses (Equations (A8b) and (A8e)) must be higher than 10 TeV to suppress this effect. Some limits on the other neutral scalar particles comes from the LEP-II experiment $M_{H_3^0} \leq 55.4$ GeV (Equation (A8d)). This time, we cannot assume the mass degeneration, and from Equations (A8g)–(A8j) it is obvious that $M_{H_1^{\pm\pm}} \neq M_{H_1^\pm}$ and $M_{H_2^{\pm\pm}} \neq M_{H_2^\pm}$. For $M_{H_1^{\pm\pm}} = 700$ GeV maximum value of $M_{H_1^\pm}$ is equal to 655 GeV, so the minimum mass gap is less than the W_1 mass: $M_{H_1^{\pm\pm}} - M_{H_1^\pm} > 45$ GeV. The $M_{H_2^\pm}$ is greater than 10 TeV (to be compared with Equation (A8b)), so we will ignore the $H_2^{\pm\pm} \rightarrow H_2^\pm + X$ decay. The whole mass spectrum and corresponding potential parameters we used in this paper are shown in the Table 2. Those values also fulfill the potential stability and unitarity bounds (see Equations (5)–(10) and (21) in [55]).

References

1. Aad, G.; Abajyan, T.; Abbott, B.; Abdallah, J.; Khalek, S.A.; Abdelalim, A.A.; Abidinov, O.; Aben, R.; Abi, B.; Abolins, M.; et al. Observation of a new particle in the search for the Standard Model Higgs boson with the ATLAS detector at the LHC. *Phys. Lett.* **2012**, *B716*, 1–29. [\[CrossRef\]](#)
2. Chatrchyan, S.; Khachatryan, V.; Sirunyan, A.M.; Tumasyan, A.; Adam, W.; Aguilo, E.; Bergauer, T.; Dragicovic, M.; Erö, J.; Fabjan, C.; et al. Observation of a New Boson at a Mass of 125 GeV with the CMS Experiment at the LHC. *Phys. Lett.* **2012**, *B716*, 30–61. [\[CrossRef\]](#)
3. Campanario, F.; Czyż, H.; Gluza, J.; Jeliński, T.; Rodrigo, G.; Tracz, S.; Zhuridov, D. Standard model radiative corrections in the pion form factor measurements do not explain the a_μ anomaly. *Phys. Rev.* **2019**, *D100*, 076004. [\[CrossRef\]](#)
4. Contino, R.; Curtin, D.; Katz, A.; Mangano, M.L.; Panico, G.; Ramsey-Musolf, M.J.; Zanderighi, G.; Anastasiou, C.; Astill, W.; Bambhaniya, G.; et al. Physics at a 100 TeV pp collider: Higgs and EW symmetry breaking studies. *CERN Yellow Rep.* **2017**, 255–440. [\[CrossRef\]](#)
5. Golling, T.; Hance, M.; Harris, P.; Mangano, M.L.; McCullough, M.; Moortgat, F.; Schwaller, P.; Torre, R.; Agrawal, P.; Alves, D.S.M.; et al. Physics at a 100 TeV pp collider: beyond the Standard Model phenomena. *CERN Yellow Rep.* **2017**, 441–634. [\[CrossRef\]](#)
6. Fukuyama, T.; Sugiyama, H.; Tsumura, K. Constraints from muon g-2 and LFV processes in the Higgs Triplet Model. *J. High Energy Phys.* **2010**, *03*, 044. [\[CrossRef\]](#)
7. Mohapatra, R.N.; Pati, J.C. A Natural left–right Symmetry. *Phys. Rev.* **1975**, *D11*, 2558. [\[CrossRef\]](#)
8. Deshpande, N.G.; Gunion, J.F.; Kayser, B.; Olness, F.I. left–right symmetric electroweak models with triplet Higgs. *Phys. Rev.* **1991**, *D44*, 837–858. [\[CrossRef\]](#)
9. Duka, P.; Gluza, J.; Zralek, M. Quantization and renormalization of the manifest left–right symmetric model of electroweak interactions. *Ann. Phys.* **2000**, *280*, 336–408. [\[CrossRef\]](#)
10. Chakraborty, J.; Ghosh, P.; Mondal, S.; Srivastava, T. Reconciling $(g-2)_\mu$ and charged lepton flavor violating processes through a doubly charged scalar. *Phys. Rev.* **2016**, *D93*, 115004. [\[CrossRef\]](#)
11. Baldini, A.M.; Bao, Y.; Baracchini, E.; Bemporad, C.; Berg, F.; Biasotti, M.; Boca, G.; Cascella, M.; Cattaneo, P.W.; Cavoto, G.; et al. Search for the lepton flavor violating decay $\mu^+ \rightarrow e^+ \gamma$ with the full dataset of the MEG experiment. *Eur. Phys. J.* **2016**, *C76*, 434. [\[CrossRef\]](#)
12. Aubert, B.; Karyotakis, Y.; Lees, J.P.; Poireau, V.; Principe, E.; Prudent, X.; Tisser, V.; Tico, J.G.; Grauges, E.; Martinelli, M.; et al. Searches for Lepton Flavor Violation in the Decays $\tau^\pm \rightarrow e^\pm \gamma$ and $\tau^\pm \rightarrow \mu^\pm \gamma$. *Phys. Rev. Lett.* **2010**, *104*, 021802. [\[CrossRef\]](#)
13. Bellgardt, U.; Otter, G.; Eichler, R.; Felawka, L.; Niebuhr, C.; Walter, H.K.; Bertl, W.; Lordong, N.; Martino, J.; Egli, S.; et al. Search for the Decay $\mu^+ \rightarrow e^+ e^+ e^-$. *Nucl. Phys.* **1988**, *B299*, 1–6. [\[CrossRef\]](#)
14. Hayasaka, K.; Inami, K.; Miyazaki, Y.; Arinstein, K.; Aulchenko, V.; Aushev, T.; Bakich, A.M.; Bay, A.; Belous, K.; Bhardwaj, V.; et al. Search for Lepton Flavor Violating Tau Decays into Three Leptons with 719 Million Produced Tau+Tau- Pairs. *Phys. Lett.* **2010**, *B687*, 139–143. [\[CrossRef\]](#)
15. Bertl, W.H.; Engfer, R.; Hermes, E.A.; Kurz, G.; Kozlowski, T.; Kuth, J.; Otter, G.; Rosenbaum, F.; Ryskulov, N.M.; Van Der Schaaf, A.; et al. A Search for muon to electron conversion in muonic gold. *Eur. Phys. J.* **2006**, *C47*, 337–346. [\[CrossRef\]](#)

16. Dinh, D.N.; Ibarra, A.; Molinaro, E.; Petcov, S.T. The $\mu - e$ Conversion in Nuclei, $\mu \rightarrow e\gamma$, $\mu \rightarrow 3e$ Decays and TeV Scale See-Saw Scenarios of Neutrino Mass Generation. *J. High Energy Phys.* **2012**, *8*, 125. [[CrossRef](#)]
17. Hisano, J.; Moroi, T.; Tobe, K.; Yamaguchi, M. Lepton flavor violation via right-handed neutrino Yukawa couplings in supersymmetric standard model. *Phys. Rev.* **1996**, *D53*, 2442–2459. [[CrossRef](#)]
18. Kitano, R.; Koike, M.; Okada, Y. Detailed calculation of lepton flavor violating muon electron conversion rate for various nuclei. *Phys. Rev.* **2002**, *D66*, 096002. [[CrossRef](#)]
19. Moore, S.R.; Whisnant, K.; Young, B.L. Second Order Corrections to the Muon Anomalous Magnetic Moment in Alternative Electroweak Models. *Phys. Rev.* **1985**, *D31*, 105. [[CrossRef](#)]
20. Leveille, J.P. The Second Order Weak Correction to (G-2) of the Muon in Arbitrary Gauge Models. *Nucl. Phys.* **1978**, *B137*, 63–76. [[CrossRef](#)]
21. Aaboud, M.; Aad, G.; Abbott, B.; Abdinov, O.; Abeloos, B.; Abidi, S.H.; AbouZeid, O.S.; Abraham, N.L.; Abramowicz, H.; Abreu, H.; et al. Search for doubly charged Higgs boson production in multi-lepton final states with the ATLAS detector using proton-proton collisions at $\sqrt{s} = 13$ TeV. *arXiv* **2017**, arXiv:1710.09748.
22. Garayoa, J.; Schwetz, T. Neutrino mass hierarchy and Majorana CP phases within the Higgs triplet model at the LHC. *J. High Energy Phys.* **2008**, *3*, 9. [[CrossRef](#)]
23. Esteban, I.; Gonzalez-Garcia, M.; Maltoni, M.; Martinez-Soler, I.; Schwetz, T. Updated fit to three neutrino mixing: exploring the accelerator-reactor complementarity. *J. High Energy Phys.* **2017**, *1*, 87. [[CrossRef](#)]
24. NuFIT. 2017. Available online: <http://www.nu-fit.org/> (accessed on 10 January 2018).
25. Sirunyan, A.M.; Tumasyan, A.; Adam, W.; Ambrogio, F.; Asilar, E.; Bergauer, T.; Brstetter, J.; Brondolin, E.; Dragicevic, M.; Ero, J.; et al. Search for a heavy right-handed W boson and a heavy neutrino in events with two same-flavor leptons and two jets at $\sqrt{s} = 13$ TeV. *J. High Energy Phys.* **2018**, *5*, 148. [[CrossRef](#)]
26. Sirunyan, A.M.; Tumasyan, A.; Adam, W.; Ambrogio, F.; Asilar, E.; Bergauer, T.; Brstetter, J.; Dragicevic, M.; Erö, J.; Del Valle, A.E.; et al. Search for heavy neutrinos and third-generation leptoquarks in hadronic states of two τ leptons and two jets in proton-proton collisions at $\sqrt{s} = 13$ TeV. *J. High Energy Phys.* **2019**, *3*, 170. [[CrossRef](#)]
27. Das, D.; Santamaria, A. Updated scalar sector constraints in Higgs triplet model. *Phys. Rev.* **2016**, *D94*, 015015. [[CrossRef](#)]
28. Bonilla, C.; Fonseca, R.M.; Valle, J.W.F. Consistency of the triplet seesaw model revisited. *Phys. Rev.* **2015**, *D92*, 075028. [[CrossRef](#)]
29. Arhrib, A.; Benbrik, R.; Chabab, M.; Moultaqa, G.; Peyranere, M.C.; Rahili, L.; Ramadan, J. The Higgs Potential in the Type II Seesaw Model. *Phys. Rev.* **2011**, *D84*, 095005. [[CrossRef](#)]
30. Krauss, M.E.; Staub, F. Unitarity constraints in triplet extensions beyond the large s limit. *arXiv* **2018**, arXiv:1805.07309.
31. Lavoura, L.; Li, L.F. Making the small oblique parameters large. *Phys. Rev.* **1994**, *D49*, 1409–1416. [[CrossRef](#)]
32. Chun, E.J.; Lee, H.M.; Sharma, P. Vacuum Stability, Perturbativity, EWPD and Higgs-to-diphoton rate in Type II Seesaw Models. *J. High Energy Phys.* **2012**, *11*, 106. [[CrossRef](#)]
33. Akeroyd, A.G.; Moretti, S. Enhancement of H to gamma gamma from doubly charged scalars in the Higgs Triplet Model. *Phys. Rev.* **2012**, *D86*, 035015. [[CrossRef](#)]
34. Shen, J.F.; Bi, Y.P.; Li, Z.X. Pair production of scalars at the ILC in the Higgs triplet model under the non-degenerate case. *EPL Europhys. Lett.* **2015**, *112*, 31002. [[CrossRef](#)]
35. Alwall, J.; Frederix, R.; Frixione, S.; Hirschi, V.; Maltoni, F.; Mattelaer, O.; Shao, H.S.; Stelzer, T.; Torrielli, P.; Zaro, M. The automated computation of tree-level and next-to-leading order differential cross-sections, and their matching to parton shower simulations. *J. High Energy Phys.* **2014**, *7*, 79. [[CrossRef](#)]
36. Rizzo, T.G. Tests of the fermion and Higgs multiplet structure of the $SU(2) \times U(1)$ model. *Phys. Rev. D* **1980**, *21*, 1404–1409. [[CrossRef](#)]
37. Czakon, M.; Gluza, J.; Jegerlehner, F.; Zralek, M. Confronting electroweak precision measurements with new physics models. *Eur. Phys. J.* **2000**, *C13*, 275–281. [[CrossRef](#)]
38. Gunion, J.F.; Grifols, J.; Mendez, A.; Kayser, B.; Olness, F.I. Higgs Bosons in left-right Symmetric Models. *Phys. Rev.* **1989**, *D40*, 1546. [[CrossRef](#)]
39. Ade, P.A.R.; Aghanim, N.; Armitage-Caplan, C.; Arnaud, M.; Ashdown, M.; Atrio-Barela, F.; Aumont, J.; Baccigalupi, C.; Banday, A.J.; Barreiro, R.B.; et al. Planck 2013 results. XVI. Cosmological parameters. *Astron. Astrophys.* **2014**, *571*, A16. [[CrossRef](#)]

40. Fileviez Perez, P.; Han, T.; Huang, G.Y.; Li, T.; Wang, K. Neutrino Masses and the CERN LHC: Testing Type II Seesaw. *Phys. Rev.* **2008**, *D78*, 015018. [[CrossRef](#)]
41. Tanabashi, M.; Hagiwara, K.; Hikasa, K.; Nakamura, K.; Sumino, Y.; Takahashi, F.; Tanaka, J.; Agashe, K.; Aielli, G.; AMSler, C.; et al. Review of Particle Physics. *Phys. Rev.* **2018**, *D98*, 030001. [[CrossRef](#)]
42. Czakon, M.; Gluza, J.; Zralek, M. Low-energy physics and left–right symmetry: Bounds on the model parameters. *Phys. Lett.* **1999**, *B458*, 355–360. [[CrossRef](#)]
43. CLIC—Compact Linear International Collider Project, CERN. Available online: <http://clic-study.web.cern.ch/> (accessed on 1 December 2019).
44. Adli, E. Plasma Wakefield Linear Colliders—Opportunities and Challenges. *Philos. Trans. R. Soc.* **2019**, *337*. [[CrossRef](#)] [[PubMed](#)]
45. Nomura, T.; Okada, H.; Yokoya, H. Discriminating leptonic Yukawa interactions with doubly charged scalar at the ILC. *Nucl. Phys.* **2018**, *B929*, 193–206. [[CrossRef](#)]
46. Dev, P.S.B.; Ramsey-Musolf, M.J.; Zhang, Y. Doubly-Charged Scalars in the Type-II Seesaw Mechanism: Fundamental Symmetry Tests and High-Energy Searches. *Phys. Rev.* **2018**, *D98*, 055013. [[CrossRef](#)]
47. Bhupal Dev, P.S.; Zhang, Y. Displaced vertex signatures of doubly charged scalars in the type-II seesaw and its left–right extensions. *J. High Energy Phys.* **2018**, *10*, 199. [[CrossRef](#)]
48. Antusch, S.; Fischer, O.; Hammad, A.; Scherb, C. Low scale type II seesaw: Present constraints and prospects for displaced vertex searches. *J. High Energy Phys.* **2019**, *02*, 157. [[CrossRef](#)]
49. Acosta, D.; Adelman, J.; Affolder, T.; Akimoto, T.; Albrow, M.G.; Ambrose, D.; Amerio, S.; Amidei, D.; Anastassov, A.; Anikeev, K.; et al. Search for long-lived doubly-charged Higgs bosons in $p\bar{p}$ collisions at $\sqrt{s} = 1.96$ TeV. *Phys. Rev. Lett.* **2005**, *95*, 071801. [[CrossRef](#)]
50. Khachatryan, V.; Sirunyan, A.M.; Tumasyan, A.; Adam, W.; Asilar, E.; Bergauer, T.; Brstetter, J.; Brondolin, E.; Dragicevic, M.; Erö, J.; et al. Search for long-lived charged particles in proton-proton collisions at $\sqrt{s} = 13$ TeV. *Phys. Rev.* **2016**, *D94*, 112004. [[CrossRef](#)]
51. Aad, G.; Abbott, B.; Abdallah, J.; Abdinov, O.; Aben, R.; Abolins, M.; AbouZeid, O.S.; Abramowicz, H.; Abreu, H.; Abreu, R.; et al. Search for heavy long-lived multi-charged particles in pp collisions at $\sqrt{s} = 8$ TeV using the ATLAS detector. *Eur. Phys. J.* **2015**, *C75*, 362. [[CrossRef](#)]
52. Aad, G.; Abajyan, T.; Abbott, B.; Abdallah, J.; Khalek, S.A.; Abdelalim, A.A.; Abdinov, O.; Aben, R.; Abi, B.; Abolins, M.; et al. Search for long-lived, multi-charged particles in pp collisions at $\sqrt{s} = 7$ TeV using the ATLAS detector. *Phys. Lett.* **2013**, *B722*, 305–323. [[CrossRef](#)]
53. Abada, A.; Abbrescia, M.; AbdusSalam, S.S.; Abdyukhanov, I.; Fernez, J.A.; Abramov, A.; Aburaia, M.; Acar, A.O.; Adzic, P.R.; Agrawal, P.; et al. FCC-hh: The Hadron Collider. *Eur. Phys. J. ST* **2019**, *228*, 755–1107. [[CrossRef](#)]
54. Pospelov, M.E. FCNC in left–right symmetric theories and constraints on the right-handed scale. *Phys. Rev.* **1997**, *D56*, 259–264. [[CrossRef](#)]
55. Chakraborty, J.; Gluza, J.; Jelinski, T.; Srivastava, T. Theoretical constraints on masses of heavy particles in left–right Symmetric Models. *Phys. Lett.* **2016**, *B759*, 361–368. [[CrossRef](#)]

